Calibration of an airborne oceanographic lidar using ocean backscattering measurements from space

JAMES H. CHURNSIDE[1,*] AND RICHARD D. MARCHBANKS[2]

[1]*NOAA Earth System Research Laboratory (ESRL) Chemical Sciences Division, 325 Broadway, Boulder, CO 80305, USA*
[2]*University of Colorado Cooperative Institute for Research in Environmental Sciences (CIRES) at the NOAA Earth System Research Laboratory (ESRL) Chemical Sciences Division, 325 Broadway, Boulder, CO 80305, USA*
*james.h.churnside@noaa.gov

Abstract: We used satellite measurements of the optical backscattering coefficient to calibrate the signal from an airborne oceanographic lidar. This technique provided the radiometric calibration for the lidar signal and a local estimate of the ratio of the particulate backscattering coefficient, b_{bp}, to the volume scattering function at the scattering angle of 180°, $\beta_p(180)$. Results using an ordinary regression, a reduced major axis regression, and a least squares bisector suggest that either of the latter two provided a better result than an ordinary regression. The statistical errors in the two recommended regressions, the difference in calibrations factors between them, and the difference between these and a laboratory calibration were all less than 5%.

1. Introduction

The backscattering coefficient of seawater, defined as the coefficient of scattering at angles > 90°, includes contributions from water and from any particles in the water. The water contribution is a weak function of water temperature and salinity [1] and has a relatively narrow range of values in the ocean. The particulate contribution, on the other hand, has a much larger range, depending on the number of particles in the water and their type.

The particulate backscatter is related to several important properties of particles in the ocean. Where the particles in the water are predominately phytoplankton, the backscattering coefficient can be related to the chlorophyll concentration [2,3]. It is also related to the concentration of particulate organic carbon [4,5]. From another perspective, it provides information on the carbon content of phytoplankton [6–8]. Where there are also significant numbers of mineral particles in the water, the backscattering coefficient can still be related to the total amount of particulate matter [9,10], although care must be taken in the interpretation, since the backscattering can be higher for mineral particles than organic particles of the same size [11].

Measurements of the particulate backscattering coefficient generally take advantage of the relatively small variability in scattering with angle at angles > 90° to obtain an estimate of the backscattering coefficient from scattering at a single angle. The relationship is particularly robust for scattering angles near 120° [12–15], and *in situ* instruments generally operate near this angle. Similarly, the effects of scattering angle can generally be neglected in passive ocean color measurements from space and the remote sensing reflectance can be related to the backscattering coefficient [16–18].

Lidar has also been used to infer the backscattering coefficient from scattering at a single angle of 180° from aircraft [19–21] and satellite [22–24]. This, however, depends on knowledge of the relationship between scattering at this angle and the backscattering coefficient, which is more variable than at 120° [12–14]. For a simple backscatter lidar, it also

depends on an absolute radiometric calibration, although this can be avoided using high-spectral-resolution lidar [20,21].

In this paper, we consider a technique to obtain the backscattering coefficient directly from lidar data by calibration against passive ocean color measurements. Preliminary results were presented at Ocean Optics XXIV [25]. The technique does not depend on retrieval of either the lidar calibration coefficient or the relationship between the volume scattering function at 180° and the backscattering coefficient, but can be used to infer both quantities. The only requirement is that the aforementioned relationship between the scattering parameters not change significantly over the area, depth range, or duration of the measurements. Once the relationship is found, it can be used where the satellite measurements are affected by clouds or vertical structure in the scattering.

2. Theory

Where the optical properties of the ocean are constant over the measurement depth range of a lidar, the signal voltage from a lidar pulse return can be expressed as [26]

$$V(z) = A_V \left[\beta_p(\pi) + \beta_w(\pi) \right] \exp(-2\alpha z) \tag{1}$$

where z is depth, A_V is a calibration factor for the output voltage, β_p is the volume scattering function of particulate scattering, β_w is the volume scattering function of scattering from seawater, and α is the attenuation coefficient.

The effects of attenuation can be removed by a linear fit to the logarithm of the signal, so that

$$V = A_V \left[\beta_p(\pi) + \beta_w(\pi) \right]. \tag{2}$$

The quality of the fit can be used as an indicator of whether or not the assumption of a uniform profile of the optical properties of the water quality is justified.

The scattering phase function from seawater is well known, with [27]

$$\beta_w(\pi) = 0.1142 b_w, \tag{3}$$

where b_w is the scattering coefficient of seawater. The scattering from seawater depends on wavelength and, to a certain extent, on temperature and salinity. We performed a fit to measurements at 546 nm made over a range of temperature, T, from 0 to 40°C and salinity, S, from 0 to 40 psu [1]. At a wavelength of 532 nm, the result is

$$b_w = 1.64 \times 10^{-3} + 1.62 \times 10^{-5} S + 1.22 \times 10^{-6} T + 1.02 \times 10^{-7} TS. \tag{4}$$

Before converting from 546 nm to 532 nm, the fit was within about 1% of the measured values.

The particulate volume scattering function can be related to the particulate backscattering coefficient, b_{bp}, by

$$\beta_p(\pi) = \frac{b_{bp}}{2\pi \chi(\pi)}, \tag{5}$$

where χ is related to the shape of the particulate phase function for scattering angles > 90°.

The lidar signal can then be expressed in terms of the backscattering coefficient as

$$V = \frac{A_V}{2\pi \chi(\pi)} b_{bp} + 0.1142 A_V b_w. \tag{6}$$

Thus, inferring the backscatter coefficient from the lidar voltage requires absolute radiometric calibration of the lidar to get A_V and knowledge of $\chi(\pi)$ and b_w. Alternatively, the relationship

can be found directly from a linear regression of lidar voltages and ocean color measurements of b_{bp}. Note that A_V often depends on a photomultiplier gain factor that is adjusted as the signal levels change. In these cases, it may be more convenient to convert the measured voltage to the corresponding photocathode current using the applied gain and the load resistance of the receiver. The equation for this case is similar:

$$I = \frac{A_I}{2\pi\chi(\pi)} b_{bp} + 0.1142 A_I b_w.$$

(7)

3. Methods

The backscattering coefficient was taken from the Moderate Resolution Imaging Spectroradiometer (MODIS) total backscattering at 531 nm from the Generalized Inherent Optical Properties (GIOP) model [28]. The Level 3 data at 4 km resolution from the Aqua and Terra satellites were used. For each lidar profile considered, we identified Aqua and Terra MODIS pixels containing the profile position on the day of the lidar flight, the day before and, the day after. Any valid backscattering values within these six satellite images were averaged together. Lidar profiles with no corresponding satellite values were not used in the analysis.

Other satellite data were used to estimate the scattering coefficient of seawater. Sea-surface temperature was obtained from the July 2015 monthly average of the MODIS Aqua Level 3 daytime 11 μ values. Sea-surface salinity was obtained from the July 2015 monthly average of Level 3 data from the Soil Moisture Active Passive (SMAP) observatory. It is based on the Combined Active-Passive (CAP) retrieval algorithm.

Lidar data were collected on ten days during the period July 8-20, 2015 off the west coast of Florida (Fig. 1). The lidar configuration used in these measurements has been described previously [19,29], but the processing was slightly different. To reduce the correlation between samples, every 25th lidar pulse was selected for consideration. This corresponds to a pulse separation on the surface of about 50 m. Since the photomultiplier gain was changed as conditions changed, the measured voltage was converted to photocathode current using the gain and the 50 Ω load impedance. The surface was identified, and a regression was performed on the logarithm of the signal between depths of 2-10 m. The exponential of the intercept was used as the signal for that lidar pulse.
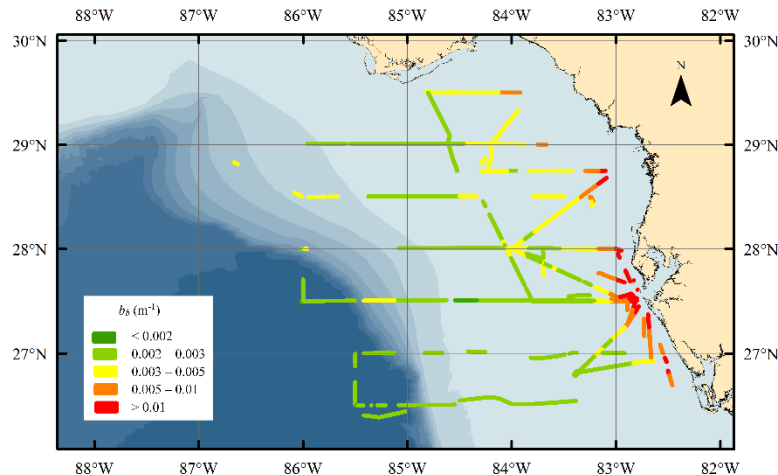

Fig. 1. Map of lidar shots color coded by the value of satellite b_b. Gaps in flight tracks are because of gaps in satellite coverage or nonuniformity in the lidar profile.

To ensure that the optical properties of the water column were uniform for the data set, we removed data where the standard deviation of the estimate of the intercept of the signal was $\sigma > 0.02$. This corresponds to an uncertainty of 2% in our estimate of the lidar signal. Examples of fits with $\sigma = 0.02$ are presented in Fig. 2. Since this was the limit, these are among the worst of the fits that were included in the analysis. These plots show the enhanced surface return produced by specular reflections from the water surface, demonstrating why 2 m was selected as the upper limit of the regression. The upper case also has return from the sea bottom at about 12 m.
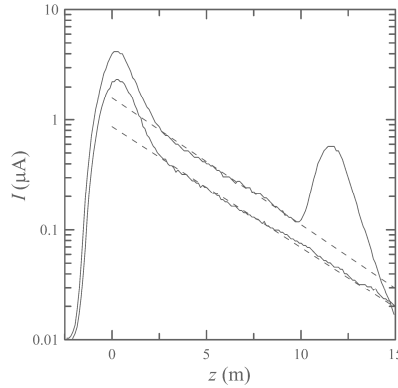

Fig. 2. Two examples of photocurrent, I, as a function of depth, z, for which the uncertainty in the intercept, $\sigma = 0.02$. Dashed lines are the regressions for $z = 2$-10 m.

4. Results

A total of 35,192 data points were selected for analysis using the criteria described above, and these are plotted in Fig. 3. The coefficient of determination, $R^2 = 0.68$. The estimated values for $\beta_w(\pi)$ did not vary much over the study area. The average value was 2.70×10^{-4} m^{-1} sr^{-1}, with a standard deviation of 2.38×10^{-6} m^{-1} sr^{-1}, and a total range of values of 2.60-2.73×10^{-4} m^{-1} sr^{-1}. From the average $\beta_w(\pi)$, the average value of b_{bw} was 1.18×10^{-3} m^{-1}. These statistics of the data do not depend on any regression, but the calibration factors inferred from them do, as seen below.
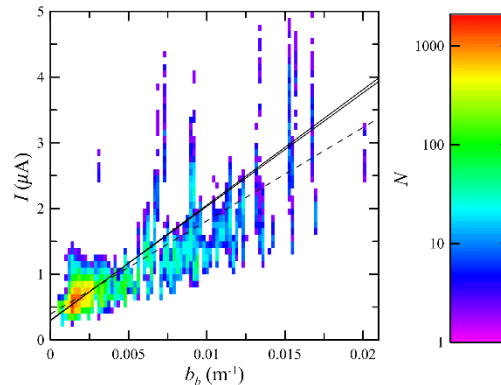

Fig. 3. Histogram plot of lidar signal current, I, as a function of MODIS backscatter coefficient, b_b, with the number of samples in each bin denoted by color according to the color bar at the right. The ordinary regression is plotted as a dashed line. The reduced major axis and least squares bisector regressions as a solid lines.

Using an ordinary regression, the best fit, plotted as a dashed line in Fig. 3, is given by

$$I = 142 \pm 1\,\mu\text{A m}\,b_{bp} + 0.393 \pm 0.003\,\mu\text{A}, \tag{8}$$

where the uncertainties in the parameters represent one standard deviation of the estimate. From the offset, we infer a calibration factor of $A_I = 1460\,\mu\text{A m}$. From this and the slope, we infer a shape parameter of $\chi = 1.63$. The root-mean-square error in b_{bp} inferred using this equation was $0.0020\,\text{m}^{-1}$.

Where there is random variability in both variables, the reduced major axis (rma) or ordinary least squares bisector (lsb) regression may be more appropriate [30]. The rma fit, plotted as a solid line in Fig. 3, is given by

$$I = 173 \pm 2\,\mu\text{A m}\,b_{bp} + 0.301 \pm 0.005\,\mu\text{A}. \tag{9}$$

Using this regression, we infer a calibration factor of $A_I = 1110 \pm 18\,\mu\text{A m}$ and a shape parameter of $\chi = 1.03 \pm 0.01$. The root-mean-square error in b_{bp} inferred using this equation was $0.0017\,\text{m}^{-1}$. The lsb fit is very similar, given by

$$I = 176 \pm 2\,\mu\text{A m}\,b_{bp} + 0.291 \pm 0.005\,\mu\text{A}. \tag{10}$$

With this regression, we obtain a calibration factor of $A_I = 1080 \pm 19\,\mu\text{A m}$ and a shape parameter of $\chi = 0.97 \pm 0.01$. The difference between these two calibration factors is 2.7% of their average value. This is similar to the combined uncertainty, given by the root mean square of 18 µA m and 19 µA m, which is 2.4% of the average of the two calibration factors.

5. Discussion

It is interesting to compare the calibration coefficient obtain by this method with that estimated from laboratory measurements. In terms of the physical parameters, the calibration coefficient can be estimated by [31]

$$A_I = \frac{\pi r^2 E T_0 T_s^2 \eta c}{2 n^3 H^2}, \tag{11}$$

where r is the receiver radius (3 cm), E is the transmitted pulse energy (100 mJ), T_O is the transmission of the receiver optics (0.16), T_S is the transmission through the sea surface (0.98), η is the responsivity of the photodetector (0.4 A W^{-1}), c is the speed of light in vacuum, n is the refractive index of sea water (1.33), and H is the distance from the lidar to the surface (height of the aircraft times the secant of lidar incidence angle, 316 m). Using these values, we get a value of $A_I = 1110\,\mu\text{A m}$, which is the same as the value inferred from the rma regression and 2.7% above the value inferred from the lsb regression. The greatest source of error in these laboratory measurements is the optics transmission. This variability was largely caused by a temperature dependence in the transmission of the interference filter. The value used in the example was measured at 22°C, but the variability at laboratory temperatures was about 20%. We should note that this filter is no longer used in our system.

There are few estimates of the shape parameter at 180°, but there have been measurements at 170°. These include values of $\chi = 0.62 \pm 0.22$ at a coastal site in the NW Atlantic [14], $\chi = 0.69 \pm 0.08$ at a coastal site in the Black Sea [32], and $\chi = 1.09 \pm 0.06$ at ten sites at coastal and open ocean locations [12]. The value we obtained from the ordinary regression is somewhat higher than would be expected from these measurements, but the rma and slb results are within the range. The rma and lsb results are however, still higher than the value of 0.5 that was used in a previous lidar study [21].

6. Conclusions

Passive ocean color measurements of backscattering coefficient can be used to calibrate lidar data such that this parameter can be inferred directly. A local relationship between the lidar

signal and the particulate backscattering coefficient was found for the eastern Gulf of Mexico, with a coefficient of determination of $R^2 = 0.68$. From this relationship, the lidar calibration coefficient and the ratio of volume scattering function to backscattering coefficient were obtained.

A reduced major axis or least squares bisector regression is recommended over an ordinary regression. These regressions provided calibration coefficients closer to laboratory measurements, χ values that were more consistent with previous measurements, and lower rms errors between the inferred and satellite measurements of backscattering coefficient.

Passive ocean color measurements in the Arctic Ocean are difficult, and space-based lidar has been suggested as a way to fill in the gaps [33–35], since it can operate in the dark and through small openings in clouds and ice. The studies have used an existing satellite lidar, but improvements will be needed to obtain vertical profiles in the Arctic [33–35]. Since the technique proposed here depends on passive ocean color measurements, it might be expected to have the same limitations. We argue that this is not the case. If sufficient passive observations can be obtained to get an accurate calibration, space-based lidar measurements can provide additional information where conditions of low sun angle, partial cloud cover, or broken ice preclude passive measurements.

References

1. K. S. Shifrin, *Physical Optics of Ocean Water*, AIP Translation Series (American Institute of Physics, 1988), p. 285.
2. Y. Huot, A. Morel, M. S. Twardowski, D. Stramski, and R. A. Reynolds, "Particle optical backscattering along a chlorophyll gradient in the upper layer of the eastern South Pacific Ocean," Biogeosciences **5**(2), 495–507 (2008).
3. R. J. W. Brewin, G. Dall'Olmo, S. Sathyendranath, and N. J. Hardman-Mountford, "Particle backscattering as a function of chlorophyll and phytoplankton size structure in the open-ocean," Opt. Express **20**(16), 17632–17652 (2012).
4. D. Stramski, R. A. Reynolds, M. Babin, S. Kaczmarek, M. R. Lewis, R. Röttgers, A. Sciandra, M. Stramska, M. S. Twardowski, B. A. Franz, and H. Claustre, "Relationships between the surface concentration of particulate organic carbon and optical properties in the eastern South Pacific and eastern Atlantic Oceans," Biogeosciences **5**(1), 171–201 (2008).
5. D. Stramski, R. A. Reynolds, M. Kahru, and B. G. Mitchell, "Estimation of particulate organic carbon in the ocean from satellite remote sensing," Science **285**(5425), 239–242 (1999).
6. J. R. Graff, T. K. Westberry, A. J. Milligan, M. B. Brown, G. Dall'Olmo, V. V. Dongen-Vogels, K. M. Reifel, and M. J. Behrenfeld, "Analytical phytoplankton carbon measurements spanning diverse ecosystems," Deep Sea Res. Part I Oceanogr. Res. Pap. **102**, 16–25 (2015).
7. M. J. Behrenfeld, E. Boss, D. A. Siegel, and D. M. Shea, "Carbon-based ocean productivity and phytoplankton physiology from space," Global Biogeochem. Cycles **19**(1), GB1006 (2005).
8. V. Martinez-Vicente, G. Dall'Olmo, G. Tarran, E. Boss, and S. Sathyendranath, "Optical backscattering is correlated with phytoplankton carbon across the Atlantic Ocean," Geophys. Res. Lett. **40**(6), 1154–1158 (2013).
9. E. Boss, L. Taylor, S. Gilbert, K. Gundersen, N. Hawley, C. Janzen, T. Johengen, H. Purcell, C. Robertson, D. W. H. Schar, G. J. Smith, and M. N. Tamburri, "Comparison of inherent optical properties as a surrogate for particulate matter concentration in coastal waters," Limnol. Oceanogr. Methods **7**(11), 803–810 (2009).
10. E. Boss, D. Stramski, T. Bergmann, W. S. Pegau, and M. Lewis, "Why should we measure the optical backscattering coefficient?" Oceanography (Wash. D.C.) **17**(2), 44–49 (2004).

11. R. A. Reynolds, D. Stramski, and G. Neukermans, "Optical backscattering by particles in Arctic seawater and relationships to particle mass concentration, size distribution, and bulk composition," Limnol. Oceanogr. **61**(5), 1869–1890 (2016).
12. J. M. Sullivan and M. S. Twardowski, "Angular shape of the oceanic particulate volume scattering function in the backward direction," Appl. Opt. **48**(35), 6811–6819 (2009).
13. X. Zhang, E. Boss, and D. J. Gray, "Significance of scattering by oceanic particles at angles around 120 degree," Opt. Express **22**(25), 31329–31336 (2014).
14. E. Boss and W. S. Pegau, "Relationship of light scattering at an angle in the backward direction to the backscattering coefficient," Appl. Opt. **40**(30), 5503–5507 (2001).
15. J.-F. Berthon, E. Shybanov, M. E. G. Lee, and G. Zibordi, "Measurements and modeling of the volume scattering function in the coastal northern Adriatic Sea," Appl. Opt. **46**(22), 5189–5203 (2007).
16. A. Morel and L. Prieur, "Analysis of variations in ocean color," Limnol. Oceanogr. **22**(4), 709–722 (1977).
17. H. R. Gordon, O. B. Brown, R. H. Evans, J. W. Brown, R. C. Smith, K. S. Baker, and D. K. Clark, "A semianalytic radiance model of ocean color," J. Geophys. Res. Atmos. **93**(D9), 10909–10924 (1988).
18. S. Maritorena, D. A. Siegel, and A. R. Peterson, "Optimization of a semianalytical ocean color model for global-scale applications," Appl. Opt. **41**(15), 2705–2714 (2002).
19. J. Churnside, R. Marchbanks, C. Lembke, and J. Beckler, "Optical backscattering measured by airborne lidar and underwater glider," Remote Sens. **9**(4), 379 (2017).
20. J. A. Schulien, M. J. Behrenfeld, J. W. Hair, C. A. Hostetler, and M. S. Twardowski, "Vertically- resolved phytoplankton carbon and net primary production from a high spectral resolution lidar," Opt. Express **25**(12), 13577–13587 (2017).
21. J. Hair, C. Hostetler, Y. Hu, M. Behrenfeld, C. Butler, D. Harper, R. Hare, T. Berkoff, A. Cook, J. Collins, N. Stockley, M. Twardowski, I. Cetinić, R. Ferrare, and T. Mack, "Combined atmospheric and ocean profiling from an airborne high spectral resolution lidar," EPJ Web of Conferences **119**, 22001 (2016).
22. X. Lu, Y. Hu, J. Pelon, C. Trepte, K. Liu, S. Rodier, S. Zeng, P. Lucker, R. Verhappen, J. Wilson, C. Audouy, C. Ferrier, S. Haouchine, B. Hunt, and B. Getzewich, "Retrieval of ocean subsurface particulate backscattering coefficient from space-borne CALIOP lidar measurements," Opt. Express **24**(25), 29001–29008 (2016).
23. X. Lu, Y. Hu, C. Trepte, S. Zeng, and J. H. Churnside, "Ocean subsurface studies with the CALIPSO spaceborne lidar," J. Geophys. Res. Oceans **119**(7), 4305–4317 (2014).
24. M. J. Behrenfeld, Y. Hu, C. A. Hostetler, G. Dall'Olmo, S. D. Rodier, J. W. Hair, and C. R. Trepte, "Space based lidar measurements of global ocean carbon stocks," Geophys. Res. Lett. **40**(16), 4355–4360 (2013).
25. J. H. Churnside and R. D. Marchbanks, "Can we use satellites to calibrate airborne lidar?" Presented at Ocean Optics XXIV, Dubrovnik, Croatia, October 8–12, 2018.
26. J. H. Churnside, "Polarization effects on oceanographic lidar," Opt. Express **16**(2), 1196–1207 (2008).
27. C. D. Mobley, *Light and Water: Radiative transfer in natural waters* (Academic, 1994), p. 592.
28. P. J. Werdell, B. A. Franz, S. W. Bailey, G. C. Feldman, E. Boss, V. E. Brando, M. Dowell, T. Hirata, S. J. Lavender, Z. Lee, H. Loisel, S. Maritorena, F. Mélin, T. S. Moore, T. J. Smyth, D. Antoine, E. Devred, O. H. F. d'Andon, and A. Mangin, "Generalized ocean color inversion model for retrieving marine inherent optical properties," Appl. Opt. **52**(10), 2019–2037 (2013).
29. J. H. Churnside and R. D. Marchbanks, "Inversion of oceanographic profiling lidars by a perturbation to a linear regression," Appl. Opt. **56**(18), 5228–5233 (2017).
30. T. Isobe, E. D. Feigelson, M. G. Akritas, and G. J. Babu, "Linear regression in astronomy. I," Astrophys. J. **364**, 104–113 (1990).
31. J. H. Churnside, "Review of profiling oceanographic lidar," Opt. Eng. **53**(5), 13 (2013).
32. M. Chami, E. Marken, J. J. Stamnes, G. Khomenko, and G. Korotaev, "Variability of the relationship between the particulate backscattering coefficient and the volume scattering function measured at fixed angles," J. Geophys. Res. Oceans **111**, C05013 (2006).
33. V. J. Hill and R. C. Zimmerman, "Estimates of primary production by remote sensing in the Arctic Ocean: Assessment of accuracy with passive and active sensors," Deep Sea Res. Part I Oceanogr. Res. Pap. **57**(10), 1243–1254 (2010).
34. J. H. Churnside and R. Marchbanks, "Sub-surface plankton layers in the Arctic Ocean," Geophys. Res. Lett. **42**(12), 4896–4902 (2015).
35. M. J. Behrenfeld, Y. Hu, R. T. O'Malley, E. S. Boss, C. A. Hostetler, D. A. Siegel, J. L. Sarmiento, J. Schulien, J. W. Hair, X. Lu, S. Rodier, and A. J. Scarino, "Annual boom–bust cycles of polar phytoplankton biomass revealed by space-based lidar," Nat. Geosci. **10**(2), 118–122 (2017).